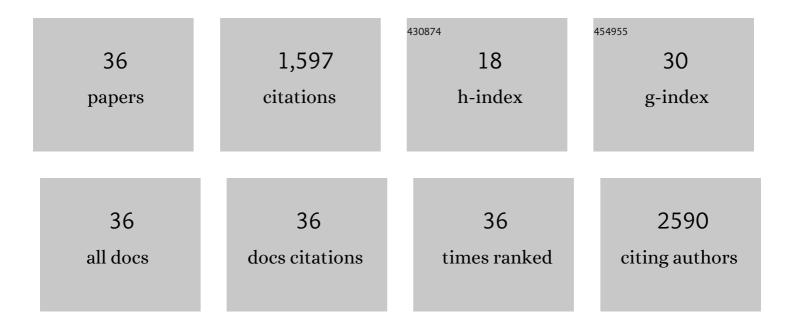
James P Carson

List of Publications by Year in descending order

Source: https://exaly.com/author-pdf/11215340/publications.pdf Version: 2024-02-01



#	Article	IF	CITATIONS
1	Enhanced anxiety and stress-induced corticosterone release are associated with increased <i>Crh</i> expression in a mouse model of Rett syndrome. Proceedings of the National Academy of Sciences of the United States of America, 2006, 103, 18267-18272.	7.1	225
2	LungMAP: The Molecular Atlas of Lung Development Program. American Journal of Physiology - Lung Cellular and Molecular Physiology, 2017, 313, L733-L740.	2.9	162
3	Comparative Computational Modeling of Airflows and Vapor Dosimetry in the Respiratory Tracts of Rat, Monkey, and Human. Toxicological Sciences, 2012, 128, 500-516.	3.1	141
4	Automated Platform for High-Resolution Tissue Imaging Using Nanospray Desorption Electrospray Ionization Mass Spectrometry. Analytical Chemistry, 2012, 84, 8351-8356.	6.5	120
5	Imaging Nicotine in Rat Brain Tissue by Use of Nanospray Desorption Electrospray Ionization Mass Spectrometry. Analytical Chemistry, 2013, 85, 882-889.	6.5	108
6	A transcriptome atlas of the mouse brain at cellular resolution. Current Opinion in Neurobiology, 2002, 12, 562-565.	4.2	78
7	High-Speed Tandem Mass Spectrometric in Situ Imaging by Nanospray Desorption Electrospray Ionization Mass Spectrometry. Analytical Chemistry, 2013, 85, 9596-9603.	6.5	69
8	Spatially-Resolved Proteomics: Rapid Quantitative Analysis of Laser Capture Microdissected Alveolar Tissue Samples. Scientific Reports, 2016, 6, 39223.	3.3	69
9	Lipidomics reveals dramatic lipid compositional changes in the maturing postnatal lung. Scientific Reports, 2017, 7, 40555.	3.3	67
10	Towards High-Resolution Tissue Imaging Using Nanospray Desorption Electrospray lonization Mass Spectrometry Coupled to Shear Force Microscopy. Journal of the American Society for Mass Spectrometry, 2018, 29, 316-322.	2.8	61
11	Fluid–structure interactions of the mitral valve and left heart: Comprehensive strategies, past, present and future. International Journal for Numerical Methods in Biomedical Engineering, 2010, 26, 348-380.	2.1	58
12	A Digital Atlas to Characterize the Mouse Brain Transcriptome. PLoS Computational Biology, 2005, 1, e41.	3.2	56
13	Wellbore cement fracture evolution at the cement–basalt caprock interface during geologic carbon sequestration. Applied Geochemistry, 2014, 47, 1-16.	3.0	50
14	Comparative Risks of Aldehyde Constituents in Cigarette Smoke Using Transient Computational Fluid Dynamics/Physiologically Based Pharmacokinetic Models of the Rat and Human Respiratory Tracts. Toxicological Sciences, 2015, 146, 65-88.	3.1	45
15	Variational generation of prismatic boundaryâ€layer meshes for biomedical computing. International Journal for Numerical Methods in Engineering, 2009, 79, 907-945.	2.8	40
16	Comparison of Two Quantitative Methods of Discerning Airspace Enlargement in Smoke-Exposed Mice. PLoS ONE, 2009, 4, e6670.	2.5	35
17	High resolution lung airway cast segmentation with proper topology suitable for computational fluid dynamic simulations. Computerized Medical Imaging and Graphics, 2010, 34, 572-578.	5.8	32
18	Phase-contrast MRI and CFD modeling of apparent 3He gas flow in rat pulmonary airways. Journal of Magnetic Resonance, 2012, 221, 129-138.	2.1	23

JAMES P CARSON

#	Article	IF	CITATIONS
19	Visualization of high resolution spatial mass spectrometric data during acquisition. , 2012, 2012, 5545-8.		20
20	An Automated Self‧imilarity Analysis of the Pulmonary Tree of the Sprague–Dawley Rat. Anatomical Record, 2008, 291, 1628-1648.	1.4	19
21	Automated measurement of heterogeneity in CT images of healthy and diseased rat lungs using variogram analysis of an octree decomposition. BMC Medical Imaging, 2014, 14, 1.	2.7	18
22	Adaptive generation of multimaterial grids from imaging data for biomedical Lagrangian fluid–structure simulations. Biomechanics and Modeling in Mechanobiology, 2010, 9, 187-201.	2.8	15
23	Landmark/image-based deformable registration of gene expression data. , 2011, , 1089-1096.		14
24	Dynamic Multiscale Boundary Conditions for 4D CT of Healthy and Emphysematous Rats. PLoS ONE, 2013, 8, e65874.	2.5	12
25	Automatic identification and truncation of boundary outlets in complex imaging-derived biomedical geometries. Medical and Biological Engineering and Computing, 2009, 47, 989-999.	2.8	10
26	In situ casting and imaging of the rat airway tree for accurate 3D reconstruction. Experimental Lung Research, 2013, 39, 249-257.	1.2	10
27	Multifunctional Activity-Based Protein Profiling of the Developing Lung. Journal of Proteome Research, 2018, 17, 2623-2634.	3.7	9
28	Markov Random Field-based fitting of a subdivision-based geometric atlas. , 2011, 2011, 2540-2547.		7
29	Spatial distribution of marker gene activity in the mouse lung during alveolarization. Data in Brief, 2019, 22, 365-372.	1.0	6
30	Automated, Foot-Bone Registration Using Subdivision-Embedded Atlases for Spatial Mapping of Bone Mineral Density. Journal of Digital Imaging, 2013, 26, 554-562.	2.9	5
31	Detecting Radiation-Induced InjuryÂUsing Rapid 3D Variogram Analysis of CT Images of Rat Lungs. Academic Radiology, 2013, 20, 1264-1271.	2.5	5
32	A chicken embryo cardiac outflow tract atlas for registering changes due to abnormal blood flow. , 2016, 2016, 1236-1239.		3
33	Lossless 3-D reconstruction and registration of semi-quantitative gene expression data in the mouse brain. , 2011, 2011, 8086-9.		2
34	Branchâ€Based Model for the Diameters of the Pulmonary Airways: Accounting for Departures From Selfâ€Consistency and Registration Errors. Anatomical Record, 2012, 295, 1027-1044.	1.4	2
35	An efficient algorithm for mapping imaging data to 3D unstructured grids in computational biomechanics. International Journal for Numerical Methods in Biomedical Engineering, 2013, 29, 1-16.	2.1	1
36	A Digital Atlas to Characterize the Mouse Brain Transcriptome. PLoS Computational Biology, 2005, preprint, e41.	3.2	0